Energy Focusing for Wireless Power Transfer in the Near-Field Region

Eleni Demarchou, Constantinos Psomas, and Ioannis Krikidis
IRIDA Research Centre for Communication Technologies,
Department of Electrical and Computer Engineering, University of Cyprus, Cyprus
e-mail: {edemar01, psomas, krikidis}@ucy.ac.cy

***Abstract*—The future sixth generation (6G) wireless communications are envisioned to bring forth the era of the Internet of Everything (IoE). This work investigates wireless power transfer (WPT) in the radiating near-field region, as a medium for charging the low-powered IoE devices. Specifically, we exploit the near-field channel model in order to create power beamfocusing at a predefined focal point. We consider a uniform planar array employing beamfocusing, and provide analytical expressions for the harvested power at the receiver located at (i) a fixed and (ii) a random location in the network. We present numerical results which validate our analysis and draw an insight overview for the near-field WPT under various design parameters while demonstrating the gains brought against far-field WPT.**

***Index Terms*—Radiating near-field, wireless power transfer, spatial randomness.**

I. Introduction

The vision towards the sixth generation (6G) wireless communications emerges the era of the Internet of Everything (IoE), where machine type connections are expected to dominate the internet traffic [1]. These connections correspond to a huge diversity of machines including, among others, devices with low-power requirements such as sensor-type equipment [2]. Powering up these devices through conventional means, might be inconvenient due to the environment's nature, the device's location, size etc. Wireless power transfer (WPT) stands out as a practical and viable solution to address the challenge of flexible charging for low-powered devices. Specifically, a device equipped with a rectifying antenna (rectenna) can harvest energy from ambient or dedicated electromagnetic radiation [3]. Due to its potentials, WPT has attracted significant interests from the research community over the recent years [4]. However, the technological advances as foreseen by the 6G vision, open the road to new opportunities [5].

The future 6G networks will exploit ultra-high frequencies including the mmWave and THz bands while utilizing large antenna arrays as a remedy to the severe path-loss attenuation [2], [6]. Under these settings, the boundary between the near-field and far-field electromagnetic regions becomes larger yielding to a significantly larger near-field radiating regime [6]. In particular, depending on the operating frequency and the array aperture, the near-field regime may expand up to hundreds of meters [7]. Different from the far-field modeling, where the channel is approximated through the planar wave assumption, in the case of the near-field regime, this approximation no longer holds and the channel is modeled based on the spherical wave assumption [8], [9]. This can be exploited for beam focusing rather than beam steering as in the far-field regime. That is, instead of steering the beam at a specific direction, operating in the near-field unlocks the ability to focus the beam on a specific location [2]. This property is exploited by the authors in [10], to facilitate multi-user downlink multiple-input multiple-output systems, while exploring various antenna architectures. Near-field communications are also investigated in [11], where the authors consider a large intelligent surface and study the uplink spectral efficiency achieved by two single-antenna users. The authors in [7], propose a phase-delay focusing in order to mitigate the near-field beam-split effect, which occurs from the extremely large bandwidth and array aperture. In [12], the authors construct beams using a carefully designed frequency modulated waveform in the spatial dimension, which mitigates the near-field misfocus effect in massive wideband phased arrays. While the investigation of the near-field technology in the communication theory is still in its infancy, the characterization of the near-field energy harvesting is also unexplored [2].

Motivated by the above, in this work we investigate the WPT in the radiating near-field regime as a medium for charging the low-powered IoE devices. We exploit the spherical wave based channel in order to focus the access point's power on a specific near-field location. Specifically, by employing maximal ratio transmission (MRT) at the transmitter, we provide analytical expressions for the harvested power at the receiver located at a fixed and a random location in the network. We present numerical results which validate our analysis and draw preliminary performance characterization of the near-field WPT under various system parameters. We show how critical the selection of the focal point is, with respect to both the access point's and the dedicated receiver's locations, in terms of harvested power and highlight the gains of near-field against far-field WPT.

II. Network Model

A. Network Topology

Consider an access point equipped with a uniform planar array consisting of N radiating elements distributed over N_x columns and N_z rows. We assume a half wavelength antenna

This work was co-funded by the European Regional Development Fund and the Republic of Cyprus through the Research and Innovation Foundation, under the projects INFRASTRUCTURES/1216/0017 (IRIDA) and CONCEPT/0521/0117 (REWIRE). This work was also supported by the European Research Council (ERC) under the European Union's Horizon 2020 research and innovation programme (Grant agreement No. 819819).

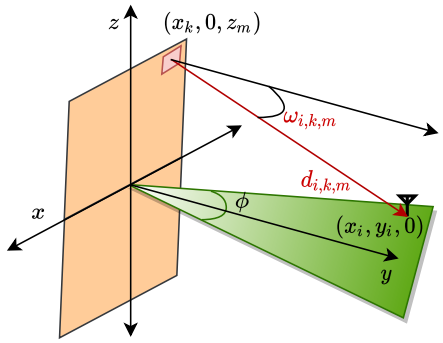

Fig. 1. A WPT network consisting of a uniform planar array and a receiver located within a sector in the near-field region.

spacing i.e., $\frac{\lambda}{2}$, thus the array aperture is expressed by $D = \sqrt{2}(\max\{N_x, N_z\} - 1)\frac{\lambda}{2}$. The access point is centered at the origin of the (x, y, z) plane such that the coordinates of the antenna element located in the k-th row and m-th column of the array are defined by $\mathbf{l}_{k,m} = (x_k, 0, z_m)$, where $x_k \in \left[-\frac{N_x-1}{2}\frac{\lambda}{2} \dots \frac{N_x-1}{2}\frac{\lambda}{2}\right]$ and $z_m \in \left[-\frac{N_z-1}{2}\frac{\lambda}{2} \dots \frac{N_z-1}{2}\frac{\lambda}{2}\right]$. We consider that the array serves a set of receivers located on the (x, y) plane, within a circular sector of radius R and angle $\phi \in [\phi_1, \phi_2]$, centered at origin towards the direction of the array. Each receiver is equipped with a rectenna and harvests energy from the access point of transmit power P. The i-th receiver is located at $\mathbf{r}_i = (x_i, y_i, 0)$ with a corresponding distance from the origin given by $\|\mathbf{r}_i\| = \sqrt{x_i^2 + y_i^2}$. The network topology is depicted in Fig. 1.

B. Channel Model

We focus on the near-field communication range; this range is determined by the physical characteristics of the array as follows. Let $d_N = \sqrt[3]{\frac{D^4}{8\lambda}}$ denote the Frensel distance indicating the minimal distance for which reactive field components from the array elements are negligible [10]. A receiver located within a distance $\|\mathbf{r}_i\| > d_N$ from the access point, is considered to lie in the radiative near-field. On the other hand, a receiver is considered to lie in the far-field regime if $\|\mathbf{r}_i\| > d_F$, where $d_F = \frac{2D^2}{\lambda}$ denotes the Fraunhofer distance [10]. In this work, we investigate the range $d_N < \|\mathbf{r}_i\| < d_F$, where the signal from the element located at $\mathbf{l}_{k,m}$ is modeled through the spherical wave assumption as follows [10]

$$g_{i,k,m} = \frac{\lambda\sqrt{E(\omega_{i,k,m})}}{4\pi d_{i,k,m}} e^{-j\frac{2\pi}{\lambda}d_{i,k,m}}, \tag{1}$$

where the subscript i refers to the i-th receiver located in the near-field regime, $d_{i,k,m}$ denotes the distance from the element located at $\mathbf{l}_{k,m}$ and is given by

$$d_{i,k,m} = \|\mathbf{r}_i - \mathbf{l}_{k,m}\| = \sqrt{(x_i - x_k)^2 + y_i^2 + z_m^2}. \tag{2}$$

Finally, $E(\omega_{i,k,m})$ denotes the radiation pattern which is a function of the angle between the element and the receiver with respect to the $y-$axis. In this work, we adopt the dipole antenna radiation pattern which is given by [10], [13],

$$E(\omega_{i,k,m}) = \begin{cases} 6\cos^2(\omega_{i,k,m}) & \omega_{i,k,m} \in [0, \pi/2], \\ 0 & \text{otherwise.} \end{cases} \tag{3}$$

III. Near-Field Wireless Power Transfer

In this section we focus on a typical receiver located at $\mathbf{r}_0 = (x_0, y_0, 0)$. Let $\mathbf{g}_i$ denote the channel vector at point $\mathbf{r}_i$, with entries $g_{i,k,m}$. We consider that the precoder at the access point employs MRT in order to focus the transmitted power on a focal point $\mathbf{r}_f$ i.e., the precoding vector is given by $\mathbf{w} = \frac{\mathbf{g}_f}{\|\mathbf{g}_f\|}$. Then the harvested power of the typical receiver at $\mathbf{r}_0$ can be expressed by [1]

$$e_0 = \frac{P\|\mathbf{g}_0{}^H\mathbf{g}_f\|^2}{\|\mathbf{g}_f\|^2}. \tag{4}$$

In the following, we consider the typical receiver located at (i) a fixed location, and (ii) a random location, and investigate the harvested power.

A. Fixed location

We first consider the typical receiver at a fixed location $\mathbf{r}_0$ with the array focusing the transmitted power at the receiver's location i.e., $\mathbf{r}_f = \mathbf{r}_0$. The harvested power at the receiver is evaluated by the following lemma.

Lemma 1. *When $\mathbf{r}_f = \mathbf{r}_0$, the harvested power is given by $e_0 = P\|\mathbf{g}_0\|^2$, where*

$$\|\mathbf{g}_0\|^2 = \frac{3\lambda^2}{8\pi^2}\sum_{k=1}^{N_x}\sum_{m=1}^{N_z}\frac{y_0^2}{\left((x_0 - x_k)^2 + y_0^2 + z_m^2\right)^2}. \tag{5}$$

Proof. See Appendix A. ∎

We now provide the following remark which follows from Lemma 1.

Remark 1. *When $\mathbf{r}_f = \mathbf{r}_0$, it can be observed from* (5)*, that when $y_0 = 0$, then the harvested power becomes zero. On the other hand, for $y_0 > 0$, the received power from the element at $\mathbf{l}_{k,m}$, is maximized when $d_{0,k,m}$ is minimized i.e., when $x_0 = x_k$. As the harvested power is obtained from the summation of the received power from each element, and since the elements are uniformly located around the origin, then e_0 is maximized at $x_0 = 0$.*

Consider now the case where the focal point of the array is at a different location from the typical receiver i.e., $\mathbf{r}_f \neq \mathbf{r}_0$. The harvested power is given in the following lemma.

Lemma 2. *When $\mathbf{r}_f \neq \mathbf{r}_0$, the harvested power at the receiver is evaluated as in* (4) *where $\|\mathbf{g}_f\|^2$ is given in Lemma 1 with the substitution of x_0 and y_0 with x_f and y_f, respectively; and the term $\|\mathbf{g}_0{}^H\mathbf{g}_f\|^2$ is given by*

$$\|\mathbf{g}_0{}^H\mathbf{g}_f\|^2 = \frac{9\lambda^4 y_0^2 y_f^2}{64\pi^4}$$

[1]The input-output relationship model adopted here is linear as the focus of this work is to investigate the near-field energy focusing. More sophisticated models for WPT are left for future work.

$$\times \sum_{k=1}^{N_x}\sum_{m=1}^{N_z}\sum_{p=1}^{N_x}\sum_{l=1}^{N_z} \frac{e^{j\frac{-2\pi}{\lambda}(d_{0,k,m}-d_{f,k,m}-d_{0,p,l}+d_{f,p,l})}}{d_{0,k,m}^2 d_{f,k,m}^2 d_{0,p,l}^2 d_{f,p,l}^2}, \quad (6)$$

where $d_{0,k,m}$, $d_{0,p,l}$, $d_{f,k,m}$ and $d_{f,p,l}$ are evaluated by (2).

Proof. See Appendix B. ∎

We now focus on the special case where $N_x = 1$ i.e., the access point located at the origin consists of one column with N_z elements with the location of the m-th element denoted by $\mathbf{l}_m = (0, 0, z_m)$. It can be obtained through Lemma 1 that when $\mathbf{r}_f = \mathbf{r}_0$, the harvested power at the typical receiver is given by

$$e_0 = P\frac{3\lambda^2}{8\pi^2}\sum_{m=1}^{N_z}\frac{y_0^2}{\left(x_0^2+y_0^2+z_m^2\right)^2}. \quad (7)$$

Note that, Remark 1 also holds for $N_x = 1$, i.e., e_0 is higher at $x_0 = 0$. Moreover, in order to compare with the case where $N_x = N_z$, let us assume that $N_x = N_z = N$ such that a total number of $N \times N$ elements are deployed. If the same number of elements are distributed over a single column, the array aperture becomes $D = \left(N^2-1\right)\frac{\lambda}{2}$. As a result, both d_N and d_F increase significantly resulting to a much larger near-field regime. On the other hand, the lowest received power at the receiver occurs from the farthest deployed element; whose distance from the receiver becomes larger as the number of elements increases. When $N_x = N_z$, the distance from the farthest element is $d_{0,N,N} = \sqrt{y_0^2 + 2(\frac{N-1}{2}\frac{\lambda}{2})^2}$. If $N_x = 1$, with the same number of elements deployed, the distance from the farthest element becomes $d_{0,0,N^2} = \sqrt{y_0^2 + (\frac{N^2-1}{2}\frac{\lambda}{2})^2}$. It follows then, that since $d_{0,N,N} > d_{0,0,N^2}$, then more power is harvested when multiple rows as well as columns are deployed such that lower distances can occur.

B. Random location

We now consider the typical receiver randomly distributed within the circular sector in order to investigate the performance of WPT over all the possible locations of the sector lying in the near filed region. In order to account for the minimum distance d_N from the access point, we consider that the receiver is randomly located within a subspace of the circular sector i.e., the area shaped by the difference of sectors with radii R and R_N, where $R > R_N \geq d_N$. To assist with our analysis we make use of the polar coordinates of $\mathbf{r}_0 = (\rho, \theta)$ where $x_0 \triangleq \rho\cos(\theta)$ and $y_0 \triangleq \rho\sin(\theta)$. Moreover, for ease of presentation, we define $\delta_{a,b} \triangleq x_a^2 + z_b^2$ to make use throughout the rest of the paper. In the following we evaluate the average harvested power at the typical receiver.

We first provide in the following proposition the harvested power for the case where $\mathbf{r}_f = \mathbf{r}_0$.

Proposition 1. *The harvested power at the typical receiver randomly located within the circular sector, when $\mathbf{r}_f = \mathbf{r}_0$, is given by*

$$e_0 = \frac{3\lambda^2 P}{8\pi^2(R^2-R_N^2)}\sum_{k=1}^{N_x}\sum_{m=1}^{N_z} f(\rho,\theta), \quad (8)$$

where

$$f(\rho,\theta) = \frac{2}{\phi}\int_{\phi_1}^{\phi_2}\int_{R_N}^{R}\frac{\rho^3\sin^2(\theta)}{\left(\rho(\rho-2x_k\cos(\theta))+\delta_{k,m}\right)^2}\,d\rho\,d\theta, \quad (9)$$

and for the special case where $\theta = \frac{\pi}{2}$,

$$f(\rho,\theta) = \frac{R_N^2}{R_N^2+\delta_{k,m}} - \frac{R^2}{R^2+\delta_{k,m}} + \ln\left(\frac{R^2+\delta_{k,m}}{R_N^2+\delta_{k,m}}\right). \quad (10)$$

Proof. See Appendix C. ∎

We now evaluate the average harvested power at the typical receiver located at $\mathbf{r}_0 = (\rho, \theta)$, for the case where $\mathbf{r}_f \neq \mathbf{r}_0$. We consider a fixed focal point at $\mathbf{r}_f$, therefore the harvested power is expressed by

$$e_0 = P\mathbb{E}\left[\frac{\|\mathbf{g}_0{}^H\mathbf{g}_f\|^2}{\|\mathbf{g}_f\|^2}\right] = \frac{P}{\|\mathbf{g}_f\|^2}\mathbb{E}\left[\|\mathbf{g}_0{}^H\mathbf{g}_f\|^2\right], \quad (11)$$

where the expectation is taken over ρ. We evaluate e_0 in the following proposition.

Proposition 2. *The harvested power at the typical receiver located at $\mathbf{r}_0 = (\rho, \theta)$, when $\mathbf{r}_f \neq \mathbf{r}_0$ is given by*

$$e_0 = \frac{9\lambda^4 y_f^2 P}{64\pi^4\|\mathbf{g}_f\|^2}\sum_{k=1}^{N_x}\sum_{m=1}^{N_z}\sum_{p=1}^{N_x}\sum_{l=1}^{Nz}\frac{e^{j\frac{2\pi}{\lambda}(d_{f,p,l}-d_{f,k,m})}}{d_{f,k,m}^2 d_{f,p,l}^2} \times \frac{2}{(R^2-R_N^2)\,\phi}\int_{\phi_1}^{\phi_2}\int_{R_N}^{R}\rho f(\rho,\theta)\,d\rho\,d\theta, \quad (12)$$

where $f(\rho,\theta)$ is given by

$$f(\rho,\theta) = \frac{\rho^2\sin^2(\theta)}{(\rho(\rho-2x_k\cos(\theta))+\delta_{k,m})} \times \frac{e^{\frac{-j2\pi}{\lambda}\left(\sqrt{\rho(\rho-2x_k\cos(\theta))+\delta_{k,m}}-\sqrt{\rho(\rho-2x_p\cos(\theta))+\delta_{p,l}}\right)}}{(\rho(\rho-2x_p\cos(\theta))+\delta_{p,l})}, \quad (13)$$

and $\|\mathbf{g}_f\|^2$ is evaluated in (5) *by substituting x_0 and y_0 with x_f and y_f, respectively.*

Proof. See Appendix D. ∎

We proceed now to the special case of $N_x = 1$ and $\theta = \frac{\pi}{2}$ such that the typical receiver is randomly distributed along the y-axis and harvests power from N_z elements distributed along the z-axis, as explained in Section II-A. With $\mathbf{r}_f = \mathbf{r}_0$, the average harvested power is evaluated similar to (7). By substituting with polar coordinates and by setting $\theta = \frac{\pi}{2}$, the harvested power at the typical receiver is evaluated as follows

$$e_0 = \frac{3\lambda^2 P}{8\pi^2}\sum_{m=1}^{N_z}\mathbb{E}\left[\frac{\rho^2}{\left(\rho^2+z_m^2\right)^2}\right] = \frac{3\lambda^2 P}{4\pi^2\left(R^2-R_N^2\right)}\sum_{m=1}^{N_z}\int_{R_N}^{R}\frac{\rho^3}{\left(\rho^2+z_m^2\right)^2}\,d\rho \quad (14)$$

$$= \frac{3\lambda^2 P}{8\pi^2\left(R^2-R_N^2\right)} \times \sum_{m=1}^{N_z}\left(\frac{R_N^2}{R_N^2+z_m^2} - \frac{R^2}{R^2+z_m^2} + \ln\left(\frac{R^2+z_m^2}{R_N^2+z_m^2}\right)\right), \quad (15)$$

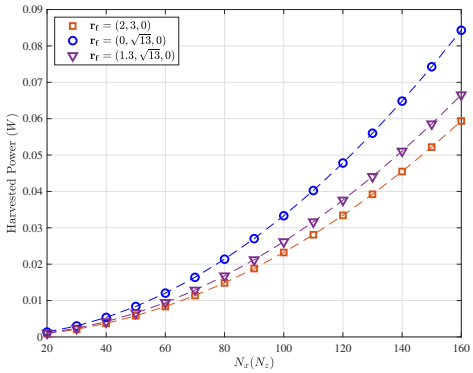

Fig. 2. Harvested power Vs antenna element per column (row) N_x (N_z); $f = 28$ GHz, $\mathbf{r}_0 = \mathbf{r}_f$, $P = 10$ W; markers and dashed lines correspond to simulation and analytical results, respectively.

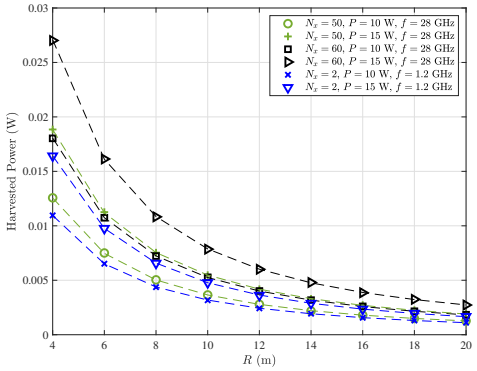

Fig. 3. Harvested power Vs R; $\mathbf{r}_0 = \mathbf{r}_f$, $R_N = 2$ m; markers and dashed lines correspond to simulation and analytical results, respectively.

where in (14) we make use of the probability density function (PDF) of ρ i.e., $\frac{2\rho}{R^2 - R_N^2}$.

IV. Numerical Results

We provide numerical results to evaluate the harvested power at the typical receiver under various network parameters. Computer simulations and analytical expressions are depicted with markers and dashed lines, respectively. Unless otherwise stated, we consider an operating frequency at $f = 28$ GHz such that $\lambda = 1.07$ cm [10].

Fig. 2 plots the harvested power e_0 with respect to the number of elements per column, where $N_x = N_z$. We plot the case where the focal point is at the receiver's location and present the performance for three locations. In all three cases we can see that the harvested power increases as the number of elements increases, which is expected as $\mathbf{r}_f = \mathbf{r}_0$. When comparing the case where $\mathbf{r}_f = (2,3,0)$ with the one where $\mathbf{r}_f = (0,\sqrt{13},0)$, we can see that while $\|(2,3,0)\| = \|(0,\sqrt{13}),0\|$, when $x_f = 0$, a better performance occurs. As explained in Remark 1, this is due to the fact that the elements are uniformly positioned around the origin, and the harvested power is obtained from the summation of the received power from each element. Similarly, we can see that when $\mathbf{r}_f = (1.3,\sqrt{13},0)$, while $\|(1.3,\sqrt{13},0)\| > \|(2,3,0)\|$ due to a smaller deviation from $x = 0$, the case where $\mathbf{r}_f = (1.3,\sqrt{13},0)$ performs better.

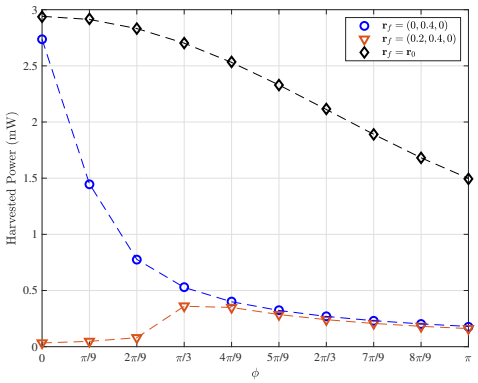

Fig. 4. Harvested power Vs sector angle ϕ; $f = 28$ GHz, $N_x = N_z = 10$, $P = 1$ W, $R_N = 0.09$ m, $R = 0.8$ m; markers and dashed lines correspond to simulation and analytical results, respectively.

In Fig. 3, we plot e_0 for the case where the receiver's location is random, $\mathbf{r}_0 = \mathbf{r}_f$ and $\theta = \frac{\pi}{2}$ such that the receiver is randomly distributed over the y-axis within the range $[R_N, R]$. We plot the harvested power with respect to R for $f = \{1.2, 28\}$ GHz, in order to compare far-field with near-field WPT [2]. For a fair comparison, we consider that the array length is constant at $L = N_x \frac{\lambda}{2}$, with $\lambda = 1.07$ cm ($f = 28$ GHz) and $N_x = \{50, 60\}$, which for the plotted range of R, correspond to the receiver being located within the near-field regime. For the far-field WPT, we consider that $N_x = \lfloor 2L/\lambda \rfloor$ with $\lambda = 25$ cm ($f = 1.2$ GHz), i.e., $N_x = 2$ [2], [10]. Clearly, the receiver harvests more power when is located within the near-field range of the array where energy focusing can be achieved. On the other hand, when $f = 28$ GHz (near-field), as R increases the receiver gets closer to the far-field regime and as a result the gain against the case where $f = 1.2$ GHz (far-field) is lower. However, in all cases e_0 decreases as R increases, since a higher R corresponds to a higher probability of the receiver being located at a larger distance form the array. Furthermore, by comparing the cases at $f = 28$ GHz, we can see that with more elements deployed or higher transmit power, a better performance is achieved.

Fig. 4 plots the harvested power for the case where the receiver is randomly distributed within a sector of angle ϕ. The sector is centered at y-axis, such that $[\phi_1, \phi_2] = \left[\frac{\pi}{2} - \frac{\phi}{2}, \frac{\pi}{2} + \frac{\phi}{2}\right]$, and the case where $\phi = 0$ corresponds to $\theta = \frac{\pi}{2}$. We plot the harvested power for $\mathbf{r}_f = \{(0, 0.4, 0), (0.2, 0.4, 0), \mathbf{r}_0\}$. As expected, the highest power is achieved when $\mathbf{r}_f = \mathbf{r}_0$, with a significant margin from the cases of fixed focal point. Furthermore, when $\mathbf{r}_f = \mathbf{r}_0$, as ϕ increases, the probability of deviating from $x_0 = x_f = 0$ becomes higher and the performance decreases. In the cases where the focal point is fixed, we can see a sharper decay of the harvested power compared to the case where $\mathbf{r}_f = \mathbf{r}_0$. This is due to the fact that, as the area of the sector increases the probability of achieving $\mathbf{r}_0 = \mathbf{r}_f$ decreases. This is more clear when $\mathbf{r}_f = (0.2, 0.4, 0)$ where the probability of achieving $\mathbf{r}_0 = \mathbf{r}_f$ is zero for $\phi_1 > \arctan\left(\frac{0.4}{0.2}\right)$ i.e., $\phi_1 > 1.107$.

V. Conclusions

In this paper, we studied the performance of WPT in the near-field region. We exploited the channel model for power focusing and by considering the typical receiver located at (i) a fixed location and (ii) a random location in the network, we provided analytical expressions for the harvested power. We presented numerical results which validated our analysis and obtained insights for various design parameters which are key for the practical applications of the near-field WPT. Specifically, our results suggest that a precise selection of the focal point towards the dedicated receiver is essential to enhance the harvested power.

Appendix

A. Proof of Lemma 1

When $\mathbf{r}_f = \mathbf{r}_0$, it follows from (4) that $e_0 = P\|\mathbf{g}_0\|^2$. For the evaluation of $\|\mathbf{g}_0\|^2$, we substitute $\cos(\omega_{0,k,m}) = \frac{y_0}{d_{0,k,m}}$ in (3), and the entries $g_{0,k,m}$ in $\mathbf{g}_0$, to get

$$\|\mathbf{g}_0\|^2 = \frac{3\lambda^2}{8\pi^2}\sum_{k=1}^{N_x}\sum_{m=1}^{N_z}\frac{y_0^2}{d_{0,k,m}^4}. \tag{16}$$

The final expression follows by substituting (2) in (16).

B. Proof of Lemma 2

For the evaluation of $\|{\mathbf{g}_0}^H\mathbf{g}_f\|^2$ we follow a similar approach as in Appendix A to get

$$\|{\mathbf{g}_0}^H\mathbf{g}_f\|^2 = \frac{9\lambda^4 y_0^2 y_f^2}{64\pi^4}\left(\sum_{k=1}^{N_x}\sum_{m=1}^{N_z}\frac{e^{-j\frac{2\pi}{\lambda}(d_{0,k,m}-d_{f,k,m})}}{d_{0,k,m}^2 d_{f,k,m}^2}\right)^2. \tag{17}$$

We then make use of the complex conjugate multiplication to expand (17) into

$$\|{\mathbf{g}_0}^H\mathbf{g}_f\|^2 = \frac{9\lambda^4 y_0^2 y_f^2}{64\pi^4}\left(\sum_{k=1}^{N_x}\sum_{m=1}^{N_z}\frac{e^{-j\frac{2\pi}{\lambda}(d_{0,k,m}-d_{f,k,m})}}{d_{0,k,m}^2 d_{f,k,m}^2}\right) \times\left(\sum_{k=1}^{N_x}\sum_{m=1}^{N_z}\frac{e^{j\frac{2\pi}{\lambda}(d_{0,k,m}-d_{f,k,m})}}{d_{0,k,m}^2 d_{f,k,m}^2}\right). \tag{18}$$

The final result is then given by evaluating the above multiplication.

C. Proof of Proposition 1

The harvested power at the typical receiver when $\mathbf{r}_f = \mathbf{r}_0$ is evaluated similar to Lemma 1. By substituting the polar coordinates in (5), we get

$$\begin{aligned} e_0 &= P\mathbb{E}\left[\|\mathbf{g}_0\|^2\right] \\ &= \frac{3\lambda^2 P}{8\pi^2}\sum_{k=1}^{N_x}\sum_{m=1}^{N_z}\mathbb{E}\left[\frac{\rho^2\sin^2(\theta)}{\left(\rho(\rho-2x_k\cos(\theta))+\delta_{k,m}\right)^2}\right], \end{aligned} \tag{19}$$

where the expectation is taken over θ and ρ. To evaluate (19) we make use of the PDFs of θ and ρ, given by $\frac{1}{\phi}$ and $\frac{2\rho}{R^2-R_N^2}$, respectively. Therefore, the harvested power is evaluated by

$$e_0 = \frac{3\lambda^2}{4\pi^2\phi(R^2-R_N^2)} \times\sum_{k=1}^{N_x}\sum_{m=1}^{N_z}\int_{\phi_1}^{\phi_2}\int_{R_N}^{R}\frac{\rho^3\sin^2(\theta)}{\left(\rho(\rho-2x_k\cos(\theta))+\delta_{k,m}\right)^2}\,d\rho\,d\theta. \tag{20}$$

For the special case where $\theta = \frac{\pi}{2}$, the expectation in (19) is taken over ρ and is evaluated by making use of the PDF of ρ similar to (20).

D. Proof of Proposition 2

Since the focal point is fixed, the term $\|\mathbf{g}_f\|^2$ is evaluated as in Lemma 1. For the evaluation of the term $\mathbb{E}\left[\|{\mathbf{g}_0}^H\mathbf{g}_f\|^2\right]$ we substitute the polar coordinates of $\mathbf{r}_0$ in (6), given in Lemma 2, and evaluate the expectation over $\mathbf{r}_0$ as follows

$$\begin{aligned} \mathbb{E}\left[\|{\mathbf{g}_0}^H\mathbf{g}_f\|^2\right] &= \frac{9\lambda^4 y_f^2}{64\pi^4} \\ &\times\sum_{k=1}^{N_x}\sum_{m=1}^{N_z}\sum_{p=1}^{N_x}\sum_{l=1}^{Nz}\frac{e^{j\frac{2\pi}{\lambda}(d_{f,p,l}-d_{f,k,m})}}{d_{f,k,m}^2 d_{f,p,l}^2}\mathbb{E}\left[f(\rho,\theta)\right], \end{aligned} \tag{21}$$

where $\mathbb{E}\left[g(\rho,\theta)\right]$ is evaluated by utilizing the PDFs of ρ and θ, as in Appendix C.

References

[1] Samsung, "6G, The next hyper-connected for all", Jul. 2020. [Online] Available: https://research.samsung.com/next-generation-communications

[2] H. Zhang, N. Shlezinger, F. Guidi, D. Dardari, M. F. Imani, and Y. C. Eldar,"Near-field wireless power transfer for 6G internet of everything mobile networks: Opportunities and challenges," *IEEE Commun. Mag.*, vol. 60, no. 3, pp. 12–18, Mar. 2022.

[3] X. Lu, P. Wang, D. Niyato, D. I. Kim, and Z. Han, "Wireless charging technologies: Fundamentals, standards, and network applications," *IEEE Commun. Surveys Tuts.*, vol. 18, no. 2, pp. 1413–1452, 2nd Quart., 2016.

[4] I. Krikidis, "Relay selection in wireless powered cooperative networks with energy storage," *IEEE J. Sel. Areas Commun.*, vol. 33, no. 12, pp. 2596–2610, Dec. 2015.

[5] W. Saad, M. Bennis and M. Chen, "A vision of 6G wireless systems: Applications, trends, technologies, and open research problems," *IEEE Network*, vol. 34, no. 3, pp. 134–142, May/June 2020.

[6] M. Cui, Z. Wu, Y. Lu, X. Wei, and L Dai, "Near-field communications for 6G: Fundamentals, challenges, potentials, and future directions", Apr. 2022. [Online] Available: https://arxiv.org/abs/2203.16318

[7] M. Cui, L. Dai, R. Schober, and L. Hanzo,"Near-field wideband beamforming for extremely large antenna arrays", Sep. 2021. [Online] Available: https://arxiv.org/abs/2109.10054

[8] P. Nepa and A. Buffi, "Near-field-focused microwave antennas: Near-field shaping and implementation," *IEEE Antennas Propag. Mag.,* vol. 59, no. 3, pp. 42–53, Jun. 2017.

[9] E. Björnson, Ö. T. Demir, and L. Sanguinetti, "A primer on near-field beamforming for arrays and reconfigurable intelligent surfaces", Oct. 2021. [Online] Available: https://arxiv.org/abs/2110.06661

[10] H. Zhang, N. Shlezinger, F. Guidi, D. Dardari, M. F. Imani, and Y. C. Eldar, "Beam focusing for near-field multi-user MIMO communications," *IEEE Trans. Wireless Commun.*, Early Access, Mar. 2022.

[11] A. d. J. Torres, L. Sanguinetti, and E. Björnson, "Near- and far-field communications with large intelligent surfaces," in *Proc. 54th Asilomar Conf. Signals, Syst., Comput.*, pp. 564–568, Pacific Grove, CA, USA, Nov. 2020.

[12] N. J. Myers and R. W. Heath, "InFocus: A spatial coding technique to mitigate misfocus in near-field LoS beamforming," *IEEE Trans. Wireless Commun.,* vol. 21, no. 4, pp. 2193–2209, Apr. 2022.

[13] S. W. Ellingson, "Path loss in reconfigurable intelligent surface-enabled channels," in *Proc. IEEE Annual Inter. Symp. Personal Indoor Mobile Radio Commun. (PIMRC)*, pp. 829-–835, Helsinki, Finland, Sep. 2021.